AIAA JOURNAL
Vol. 39, No. 2, February 2001

Sensitivity Study of Precision Pressurized Membrane Reflector Deformations

G. Greschik*
University of Colorado, Boulder, Colorado 80309-0429
A. Palisoc,† C. Cassapakis,‡ and G. Veal§
L'Garde, Inc., Tustin, California 92680-6487
and
M. M. Mikulas¶
University of Colorado, Boulder, Colorado 80309-0429

Geometric tolerances for precision reflectors are much more stringent than for traditional structures. This makes the reliability of their design critical whenever test verification is difficult, as in the case of space inflatable reflectors. However, the accuracy of pressurized film shape predictions can be degraded by many factors, which are often not sufficiently recognized. To show the importance of details in precision membrane analysis, the sensitivity of membrane shapes to selected environmental effects and physical assumptions used in numerical modeling is illustrated. In particular, 1) film thickness and material property variations, 2) thermal effects and support perturbations, and 3) the modeling of wrinkling are considered. Errors from inappropriately accounting for the preceding in the prediction of parabolic reflector shapes are compared to typical reflector tolerances. The main contribution of this study to the wealth of previous work on membrane structures is to demonstrate the practical importance of the preceding effects in current industrial practice. Another contribution is the development of a simple, high-precision, and robust numerical tool for axisymmetric membrane analysis.

Nomenclature

E, ν	=	Young's modulus, Poisson's ratio
e_{eu}, ϵ_{eu}	=	Euclidean surface error norm and tolerance
f	=	paraboloid focal length
p	=	pressure
R, D	=	radius and diameter
R_0	=	radius of zone unaffected by support displacements
r, z	=	radial and axial coordinates
s	=	arc length along axisymmetric membrane contour
t	=	membrane thickness
α	=	meridian slope angle, $\tan^{-1}(\mathrm{d}z/\mathrm{d}r)$
ε	=	engineering strain, $(l - l_I)/l_I$
κ	=	meridian curvature, $\mathrm{d}\alpha/\mathrm{d}s$
σ, N	=	stress and stress resultant

Subscripts

c, m	=	reference to circumferential and meridional directions
ctr	=	reference to membrane center
I	=	reference to strain-free state

Introduction

PRESSURIZED membranes have been considered, designed, and used for space applications throughout the space age.[1] However, for high-precision applications such as radio frequency (rf) or optical reflectors their advantages of deployment simplicity and low-volume storage have been offset by sensitivity to environmental effects, difficulty of shape control, and a lack of confidence. It is only recently[2] that economic pressure and advances in material technology renewed interest in precision space film applications. It is this current and practical interest that motivated the present work.

Previous Work

Perhaps the first publication to address a membrane problem without a primary focus on shells, Hencky's 1915 work on the approximate solution of a homogeneous isotropic linear elastic circular membrane under lateral load[3] is one of the first achievements of the distinct engineering discipline of membrane structures. Since then, the literature on membrane theory, analysis and solution techniques, and application engineering has grown immense. No attempt is made here to generally review this plethora of work. (For an overall review the reader is referred to Libai and Simmonds.[4]) Rather, we focus on reflector engineering and highlight trends of literature relevant to the present work via selected references.

Shape prediction sensitivity is herein discussed assuming axisymmetry, in line with much of the literature.[3,5–9] Although the relative simplicity of the axisymmetric governing equations could explain this trend for theoretical contributions, numerical studies[8,9] also often address this class of problems despite that general numerical solution techniques and their theory are not necessarily so limited.[10–12] The reason for this bias is that axisymmetric membrane applications abound. They include many balloons,[8] parachutes,[13] air bags,[14] and reflectors: the application of concern herein.

Although the results discussed next may be useful in the design of general membrane domes, they are restricted to paraboloids—the shape most often required of communication and scientific reflectors. This geometry raises two immediate design questions. In particular, 1) how well can an initially flat pressurized membrane approximate a paraboloid, and 2) how to design a membrane that pressurizes into an exact paraboloid. Many studies of flat membrane pressurization (including experimental work[15]) are associated with the former question. Of special interest of these are Refs. 7 and 16, which also address how film properties (such as thickness) must vary and what the support conditions should be for a flat film to produce a paraboloid under pressure. The problem of initial shape design for a desired pressurized geometry is simple for axisymmetry because the problem is statically determinate.[17,18] However, the sensitivity of predictions to modeling approximations, addressed in the present paper, is a pivotal practical concern, which is often overlooked.

Received 12 April 1999; revision received 7 June 2000; accepted for publication 26 June 2000.

*Research Associate, C.Box 429, Center for Aerospace Structures; greschik@colorado.edu.
†Structural Engineer, 15181 Woodlawn Avenue; art_palisoc@lgarde.com.
‡President, 15181 Woodlawn Avenue; costa_cassapakis@lgarde.com.
§Vice President of Operations, 15181 Woodlawn Avenue; gordon_veal@lgarde.com.
¶Professor of Aerospace Engineering, C.Box 429, Center for Aerospace Structures; mikulas@colorado.edu.

The results presented next demonstrate well that the influence of the perturbations of edge supports can be highly localized to the support's vicinity. This localization is often referred to as edge or boundary-layer effect and has been studied before.[19,20] The present results offer a practical perspective of this phenomenon.

The significance of wrinkling in membrane modeling is given special attention next. For a typical structural problem where macroscopic membrane behavior is of interest, the details of the wrinkles are insignificant. Accordingly, the membrane can be modeled via a smooth (i.e., unwrinkled) pseudosurface, and the extent of wrinkling can be measured by the average excess compressive strain compared to that coming from the membrane's constitutive response in the zero principal stress direction. This measure can be incorporated into the formulation via the constitutive model, e.g., through the Poisson's ratio,[21] or it can be used as an explicit strain measure.[22] However, this extra variable does not need to be used for the solution of a wrinkled membrane problem. This is the case for the present work where, rather than explicitly introducing a new variable or incorporating it into a constitutive parameter, the general set of constitutive laws is replaced with a reduced set when wrinkling occurs.

Motivation

Despite the abundance of references on membrane analysis and theory, the significance of 1) environmental effects, 2) certain physical assumptions in the engineering model, and 3) mathematical details of the model formulation in pressurized reflector shape prediction are not appreciated sufficiently in the space engineering community. The authors' observations include attempts to benchmark nonlinear FEM results to approximate or empirical solutions associated with unknown errors, accepting results of FEM programs not equipped to model wrinkling even if (localized) compressive stresses are produced, misinterpreting how reflector surface accuracy should be measured, and a lack of appreciation of the sensitivity of numerical results to modeling and physical details.

One reason for such oversights may be the limited familiarity with precision reflector design and with membrane engineering by some structural engineers. The shape prediction of precision membrane structures requires the analyst to be keenly aware of two facts. First, optical and rf devices are associated with tolerances much more stringent than load bearing structures: geometric errors of a fraction of a millimeter can render an optical device inoperable. Second, membranes can be much more sensitive than stiffer structures to a variety of perturbations. The awareness of these two factors is all of the more necessary in space engineering, where tests of shape predictions can be prohibitively difficult.

The recognition of the sensitivity of membrane analyses is quite limited because very few publications address the quantitative, practical aspects of membrane engineering. The authors are aware of only one such work that compares the accuracy of analytical shape prediction based on variational principles for solar concentrators[23] formed from initially flat membranes. (This work is based on heliostat accuracy tolerances and a surface error derived from meridian slope errors—a metric not compatible with wavefront error-based rms measures meaningful for rf applications.[24]) No similar work for precision reflectors is available. The present study contributes to filling this void.

Present Contribution

Recognizing the gap between the needs of precision membrane engineering and engineering practice, a study was conducted to demonstrate how some modeling approximations, engineering assumptions about the physical nature of a problem, and environmental effects affect the reliability of shape predictions for membrane reflectors.[17,18] The study considered the precision required of current applications in various environments. It also reviewed existing theoretical and empirical formulas and modeling approximations, the use and abuse of which the authors have observed. The present paper summarizes those results of this study that are directly relevant to engineering with standard numerical tools. In particular, we address 1) the effects of film thickness and material property variations, 2) the impact of thermal effects and support perturbations, and 3) the modeling of wrinkling using full geometric nonlinearities but a linear elastic constitutive model. The influence on the computed shape of each effect considered is studied for several membrane domes with the software package AM[17,18] (Axisymmetric Membrane) by comparison with unaltered reference solutions. It is shown that the errors caused by neglect in the preceding effects can be unacceptable for precision membrane engineering.

For the proper evaluation of the comparisons below and for the more detailed study of engineering and theoretical approximations from which the present results are selected,[17,18] the numerical accuracy of the analysis results have been crucial. However, the consequent striving for accuracy in our formulation does not imply a belief that minimizing numerical or mathematical approximations guarantees good agreement between prediction and reality. Prediction errors have many reasons, including constitutive models, which are less than perfect reflections of true material behavior, idealized distributions of properties and geometry instead of the statistically disturbed real patterns, manufacturing errors, etc. Here we simply focus on a few of these factors that can be easily addressed in design, and we demonstrate the impact of these alone with an accuracy compatible with the technical needs of rf and optical applications.

The optical accuracy of these applications has been the motivation behind the elimination of mathematical approximations and the painstaking minimization of numerical errors in AM. In fact, besides the demonstration of shape sensitivity a secondary contribution of the present work is AM itself. Beyond its role in the present study, AM also proved to be a handy tool for preliminary design (when even reflectors with gores can often be modeled as axisymmetric).

To first outline the technical context and to clarify some of the terminology, we begin with a review of the so-called rms surface error for rf and optical reflectors. A summary of axisymmetric membrane mechanics follows via a discussion of the formulation embedded in AM. Finally, the set of test problems and studied effects are introduced, and the results are presented and discussed.

Surface Errors

The error in a predicted membrane shape will be measured by the Euclidean norm

$$e_{\text{eu}} = \left[\int (\Delta z)^2 \frac{\mathrm{d}A}{A} \right]^{\frac{1}{2}} \tag{1}$$

where Δz is the axial error between the compared—typically, the ideal and the corrupted—surfaces, A is their axial projection (the aperture for a reflector), and their relative position is adjusted to minimize e_{eu}. This is not the so-called rms error e_{rms} associated with rf and optical applications. However, we cannot use e_{rms} because the studied problems also include initially flat membranes that do not inflate to optical shapes.

The radiometric rms error is defined only for optical (reflector) shapes[24] as

$$e_{\text{rms}} = \left[\int \left(\frac{\Delta l}{2} \right)^2 \frac{\mathrm{d}A}{A} \right]^{\frac{1}{2}} \tag{2}$$

where Δl is the wave-front error (the path-length change suffered as a result of surface imperfections by a reflected ray of radiation) and A is the reflector aperture. The significance of e_{rms} is that it enables one to estimate the gain loss of a reflector caused by minor surface errors as

$$G/G_0 = \exp\left(-[4\pi e_{\text{rms}}/\lambda]^2\right) \tag{3}$$

where G and G_0 are the gains associated with the actual and ideal surfaces and λ is the wavelength. For example, for an $f = 28$ GHz frequency ($\lambda = 10.7$ mm), which is representative of some currently considered applications, a 2-dB loss of antenna gain corresponds to an rms error of $e_{\text{rms}} = (0.2\,\ell n\,10)^{1/2}\lambda/(4\pi) \approx 0.58$ mm.

For a shallow parabolic reference surface the wave-front error in Eq. (2) can be approximated as $\Delta l = (2\Delta z \cos^2 \alpha)$, where Δz is the axial deviation from and α is the angle of meridian slope of the paraboloid. Further assuming $\cos\alpha = 1$ reduces Eq. (2) to Eq. (1): e_{eu} approaches e_{rms} for shallow parabolic dishes. This makes the results of the present study radiometrically meaningful (despite the use of e_{eu}) for shallow parabolic dishes. To help the practical

assessment of the errors discussed later, a guideline error tolerance ϵ_{eu} will be established.

As the position of optical elements in a device is adjusted after the fabrication of the elements (fabrication involves pressurization for a membrane reflector), reflector surface design is primarily concerned with surface shapes, as opposed to the precise position of those shapes in space. Accordingly, the errors Δz and Δl in expressions Eqs. (1) and (2) are measured after axially positioning one of the compared surfaces to minimize the resulting integrals.

Engineering judgment suggests that, to design for a particular precision, an analysis tool should be an order of magnitude more accurate. Thus the $e_{rms} \approx 0.58$ mm representative reflector precision just derived requires an $e_{rms} \approx 0.06$ mm shape prediction accuracy. Because $e_{eu} > e_{rms}$ for a parabolic reference surface,[24] a required shape prediction tolerance of $\epsilon_{eu} = 0.1$ mm is taken here as a guideline.

There is much confusion in the structural engineering community caused by referring indiscriminately to many Euclidean (root-mean-square) error norms similar to Eq. (1) as the rms error. Although such norms can generally quantify surface errors and their use may be necessitated by nonoptical reference surfaces (as now), they should always be carefully distinguished from the radiometric rms error.

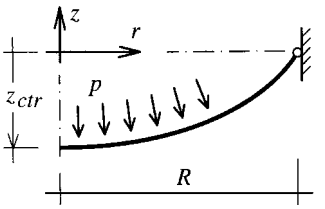

Fig. 1 Membrane contour.

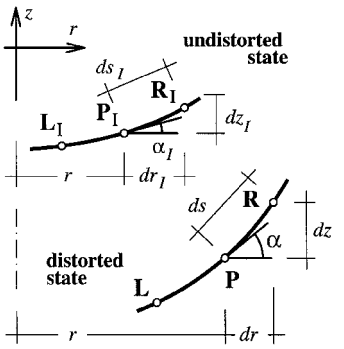

Fig. 2 Geometry of deformations.

Axisymmetric Membrane Formulation

Of several mathematically equivalent fully geometric nonlinear formulations for axisymmetric membranes, the one described in the following was adopted for the present work (and incorporated in the software package AM[18]) because of numerical accuracy, programming simplicity, streamlining of details for future program extensions, and computational efficiency. As most elements of this formulation are widely used, no references are cited for these, and only nonstandard features are commented upon.

Governing Equations

Consider the meridian of the axisymmetric membrane (Fig. 1) in radial and axial coordinates r and z. The deformation of this contour under pressure and some key geometric variables are shown in Fig. 2. The geometric quantities associated with this deformation are

$$\varepsilon_c = \frac{r}{r_I} - 1 \tag{4}$$

$$\varepsilon_m = \frac{\mathrm{d}s}{\mathrm{d}s_I} - 1 \tag{5}$$

$$\kappa = \frac{\mathrm{d}\alpha}{\mathrm{d}s} \tag{6}$$

$$\frac{\mathrm{d}r}{\mathrm{d}s} = \cos\alpha \tag{7}$$

$$\frac{\mathrm{d}z}{\mathrm{d}s} = \sin\alpha \tag{8}$$

where the function $z(r)$ describes the (pressurized) contour. For full geometric nonlinearity none of the expressions in Eqs. (4–8) are simplified.

Any other strain can be expressed in terms of the preceding engineering strains. Such strains may always be introduced into the constitutive relations if needed.

The axial equilibrium of a membrane cap of radius r and local equilibrium in the surface normal direction at point $z(r)$ entail

$$pr = 2N_m \sin\alpha \tag{9}$$

$$p = N_m\kappa + N_c\kappa_c \tag{10}$$

where

$$\kappa_c = \sin\alpha / r \tag{11}$$

is the surface curvature in the circumferential direction and N_m and N_c are the radial and circumferential membrane stress resultants per unit deformed length (true, Cauchy-type, membrane forces). These relations are convenient because the curvature κ, key to the meridian integration engine developed, can easily be expressed from Eq. (10).

To overcome the singularity at the apex ($r = 0$) of relations Eqs. (9) and (10), they are there replaced with

$$N_m = N_c \tag{12}$$

$$p = 2N_m\kappa \tag{13}$$

Numerical testing revealed no convergence or accuracy problems in the vicinity of the singularity.

The formulation is completed by the constitutive relations defined in terms of the engineering strains ε_m, ε_c and the Cauchy-type membrane forces N_m, N_c. In case of linear elasticity (the constitutive module written for AM for the present study), these equations are

$$Et\varepsilon_c = N_c(1 + \varepsilon_m) - \nu N_m(1 + \varepsilon_c) \tag{14}$$

$$Et\varepsilon_m = N_m(1 + \varepsilon_c) - \nu N_c(1 + \varepsilon_m) \tag{15}$$

where the $(1 + \varepsilon)$ terms translate the Cauchy-type stress resultants into Piola–Kirchoff-type ones (standard material testing measures the elastic constitutive constants in the context of the latter). The distinction between Cauchy and Piola–Kirchoff quantities is made in order to improve accuracy despite that a linear elastic material formulation is limited to small strains. (This is also the case for quality commercial FEM codes such as MSC NASTRAN, where the Jacobian of the deformation tensor is used to properly convert strain measures in a geometric nonlinear analysis even if a linear elastic constitutive relation is used.)

It is possible to obtain compressive stress(es) by the solution of Eqs. (14) and (15) for certain strain values. However, instead of developing such stresses, a membrane wrinkles—in the circumferential direction, in case of an axisymmetric pressurized canopy. Denoting the associated circumferential strain caused by Poisson contraction as $\varepsilon_{c,\mathrm{elast}}$ and the excess compressive strain caused by wrinkling as ε_w, the stress-strain relation in the wrinkled state can be written as

$$N_c = 0 \tag{16}$$

$$N_m(1 + \varepsilon_c) = Et\varepsilon_m \tag{17}$$

where $\varepsilon_c = \varepsilon_{c,\mathrm{elast}} + \varepsilon_w$. [Via Eqs. (9–11) this entails $\kappa = 2\kappa_c$, which is the geometric definition of the contour of the wrinkled region, the parachute curve.[13]]

At the onset of wrinkling signaled by compressive stresses from Eqs. (14) and (15), these linear elastic constitutive relations are replaced with those reflecting the wrinkled state [Eqs. (16) and (17)].

Further, nonlinear, constitutive models are also available in the literature and could be included in the formulation. However, such models are rarely used for pressurized canopy design in the aerospace industry. For direct relevance to industrial practice, therefore, here only linear elasticity is considered.

AM and Its Solution Strategy

AM, the software package developed for the present study, is based on the formulation outlined in the preceding section. The development of this code was necessary because standard numerical tools applicable to membrane analysis (commercial FEM codes such as NASTRAN) are cumbersome and can overcome numerical problems associated with membrane analysis often only with special assistance or nonstandard modeling options. For the hundreds of analyses from which the results below are selected, a tool to prepare and solve axisymmetric membrane problems within minutes was needed. The ability to model wrinkling, not readily available in most commercial codes, was also required as well as the potential for the easy incorporation of nonlinear constitutive relations for future work. Further, the assessment of prediction errors caused by assumptions used in approximate solutions (discussed elsewhere[17]) was also required.

At the heart of AM is an integrator to solve the meridian as an initial value problem from any known point onward. In each integration step along the discretized contour, the state and position of a point **R** is iteratively determined from the known adjacent point **P** (cf. Fig. 2) with Eqs. (4–17) satisfied. (Which of the alternative elements of the governing equations to use is decided point by point.) The previous point **L** is used, if available, only for the predictor step of this iteration.

The meridian is repeatedly integrated (inward from the perimeter or outward from the apex) with the initial values varied until the boundary conditions on the other end are satisfied with acceptable accuracy. The numerical details have been developed and tuned with painstaking care to minimize solution errors. Robustness has been maintained by a recursive strategy whereby, if the contour integration failed to converge (successfully complete) even after its initial value was refined to exhaust computer numerical precision, the solution was restarted from an appropriately chosen location along the properly solved part of the contour.

AM's computational engine has been carefully verified[17] against 1) MSC NASTRAN, 2) an inverse solver also included in AM, and 3) pressurized spherical membrane problems. Initially flat membrane results in the limit (for diminishing loads) were also compared with Hencky's approximate solution.

Problem Specification

The sensitivity of shape prediction to selected effects is demonstrated next for a number of initially curved membranes that pressurize to exact paraboloids and for the limit case of initially flat shapes without prestress. Half-mil Kapton film is used [$t = 0.0127$ mm, $E = 5.516$ GPa (=800 ksi), $\nu = 0.3$, and coefficient of thermal expansion $= 1.2 \times 10^{-5}$]. The pressurized aperture radii are $R = 1.5$ m. (The stress-free membrane diameter differs from the pressurized one if the membrane is initially curved and pressurizes into a paraboloid.[17])

For initially nonflat membranes designed to pressurize to exact paraboloids, f/D (focal-length-to-diameter) ratios of 0.25, 0.50, 0.75, 1.0, 1.5, 2.0, and 4.0 are discussed. For each of these models and also for initially flat ones, pressures to produce skin stresses σ_{ctr} of 0.8618, 1.723, 3.447, and 6.895 MPa at the apex are considered. These load cases are referred to as 125, 250, 500, and 1000, which are the skin stresses in pounds per square inch. The ranges presented extend beyond practical interest to better reveal trends and to provide a gradual transition between the parabolic shapes and the flat membrane.

The pressure to be applied to a canopy for a particular skin stress at the apex depends on the shape and size of the membrane. For initially flat shapes the four applied pressures were determined with AM as $p = 0.322$, 0.911, 2.577, and 7.285 Pa (1 psi $\approx$ 6894.8 Pa), respectively. For parabolic shapes they can be calculated from the pressurized contour via Eq. (13) as $p = t\sigma_{\text{ctr}}/f$.

Our choice to define the load cases with particular values of skin stress, rather than of applied pressure, serves the scalability of the results, including surface errors e_{eu}, without changing the membrane thickness. (Film thicknesses for many space structures cannot be decreased further because they already approach the limits of manufacturability and quality control. Consequently, scaling has to be limited to the overall structural geometry, leaving the film thicknesses unchanged. This constraint prohibits the use of the classical replica scaling laws, which relate to the adjustment of all aspects of the structural geometry. Instead, the recently developed rules for constant thickness scaling[25,26] need to be used. These relations maintain the same skin stress for all model sizes.)

For all analyses a meridian discretization to 250 near-equal integration steps has been used. The iterative solution of the meridian was governed by the meridional membrane force at one endpoint of the contour—the initial value of the contour integration. The error in the radial position of the other end of the contour was required to diminish below $\epsilon_R = 10^{-13}$ times the model radius. When the outlined solution scheme was embedded in a global iteration to achieve a given skin stress at the apex, the error tolerance for the embedding iteration was $\epsilon_\sigma = 10^{-8}$ times the target stress.

Parametric Study

Surface errors are presented next in a normalized form $e = e_{\text{eu}} \times 10^4/R$. The guideline shape prediction tolerance $\epsilon_{\text{eu}} = 0.1$ mm just established corresponds to an $\epsilon_{\text{norm}} = \epsilon_{eu} \times 10^4/R = 0.1 \times 10^4/1500 \approx 0.7$ normalized tolerance for a 3-m-diam reflector.

Film Property Nonuniformities

In general, the material properties and thickness of a film are not uniform, and even their averages may differ significantly from the design specifications. Such deviations may involve a systematic bias within the structure as a result of the properties of the roll of film from which the gores are cut and the uniform orientation of the gores on the roll. Consider two distributions of a 5% deviation between the nominal (modeled) and true film thicknesses: 1) a uniform 5% increase and 2) a variation linear with the radius from a 5% thickness increase at the center to a 5% decrease at the perimeter. The normalized errors of shape predictions based on the nominal values are shown in Table 1. Observe the following:

1) Generally, the shallower a shape is, the greater the errors.

2) The errors increase with increasing pressure levels.

3) Nonuniform thickness perturbations have a more benign effect than uniform ones, and they reflect the preceding trends less.

The $\epsilon_{\text{norm}} = 0.7$ guideline tolerance for 3-m-diam reflectors is violated for a number of models. Similar results are expected from like variations of the elastic modulus.

Temperature Loads

Consider temperature changes of 50°C (which is much below typical values in a space environment) with distributions similar to the thickness variation just stated, namely; $\Delta T = 50$°C and

Table 1 Normalized shape prediction errors $e = (e_{\text{eu}} \times 10^4/R)$ as a result of thickness variations (no target f/D ratio identifies the initially flat membranes)

f/D	0.25	0.50	0.75	1.0	1.5	2.0	4.0	n/a[a]
				Load case 125				
$t5\%+$[b]	0.1	0.1	0.1	0.1	0.2	0.3	0.4	0.6
$t5\%\pm$[c]	0.1	0.1	0.1	0.1	0.1	0.1	0.1	0.1
				Load case 250				
$t5\%+$	0.1	0.1	0.2	0.3	0.3	0.5	0.6	0.8
$t5\%\pm$	0.1	0.1	0.1	0.1	0.2	0.2	0.1	0.2
				Load case 500				
$t5\%+$	0.3	0.3	0.4	0.5	0.7	0.9	1.1	1.1
$t5\%\pm$	0.3	0.2	0.3	0.3	0.3	0.3	0.3	0.3
				Load case 1000				
$t5\%+$	0.6	0.6	0.8	1.0	1.3	1.2	1.9	1.5
$t5\%\pm$	0.5	0.4	0.4	0.4	0.4	0.3	0.5	0.3

[a] n/a, Not applicable.
[b] $t5\%+$: membrane thickness t uniformly increased to $1.05t$.
[c] $t5\%\pm$: t varied from $1.05t$ at the center to $0.95t$ at the edge.

Table 2 Normalized shape prediction errors $e = (e_{eu} \times 10^4/R)$ caused by thermal loads (no target f/D ratio identifies the initially flat membranes)

f/D	0.25	0.50	0.75	1.0	1.5	2.0	4.0	n/a[a]
				Load case 125				
$T50+$[b]	5.9	8.0	11	14	20	25	40	47
$T50\pm$[c]	3.9	5.6	7.3	9.3	11	13	13	17
				Load case 250				
$T50+$	5.9	8.0	11	14	19	24	27	38
$T50\pm$	3.8	5.3	6.7	8.0	10	10	12	14
				Load case 500				
$T50+$	5.9	8.0	11	14	19	23	28	30
$T50\pm$	3.6	4.9	6.1	6.7	7.3	7.3	9.3	10
				Load case 1000				
$T50+$	5.9	8.0	11	13	17	17	25	29
$T50\pm$	3.4	4.4	5.1	5.3	5.1	4.5	6.7	3.5

[a] n/a, Not applicable.
[b] $T50+$: temperature T uniformly increased to $T + 50°C$.
[c] $T50\pm$: T varied from $T + 50°C$ at the center to $T - 50°C$ at the edge.

$\Delta T = (1 - 2r/R) \times 50°C$. The shape prediction errors from not modeling these loads are tabulated in Table 2. Observe the following:

1) The considered temperature loads degrade prediction accuracy much more severely than the thickness variations.

2) Generally, the shallower a shape is, the greater the errors.

3) The errors weakly decrease with increasing pressure.

4) Nonuniform temperature loads are more benign than uniform ones.

All errors are above the $\epsilon_{norm} = 0.7$ guideline tolerance for $D =$ 3-m reflectors.

The membrane dilation from a uniform temperature load distorts the shape primarily because of the lack of compatible perimeter displacements. Thus the mechanical effect of a uniform temperature differential and a perimeter displacement are similar, and the discussion of the effects of the latter to follow also applies to uniform temperature loads.

Boundary-Layer Effect

Although the overall error between shapes undisturbed and disturbed by uniform temperature loads (or perimeter displacements) is generally significant (cf. Table 2), such perturbations tend not to alter the shape of the central region of initially curved membranes. This localization of distortions to the vicinity of the support, the edge effect or boundary-layer effect,[19,20] can protect the shape of the center from the perturbation. To study this phenomenon, the support has been radially displaced with eight increments of $\Delta R/R = 3 \times 10^{-4} = 0.03\%$ in each of the positive and negative directions (steps of $\Delta R = 0.45$ mm for the 3-m-diam models $\Delta R = -3.6$ mm $\rightarrow +3.6$ mm) for all shapes and load cases. Each increment corresponds to a 25°C temperature step.

Stress boundary layers for an $f/D = 1$ membrane paraboloid are illustrated in Figs. 3 and 4 because of out- and inward perimeter perturbations of 2.7 mm—±150°C temperature loads—for load case 125. (The displacement and length information is nondimensionalized, but the stresses are not, to comply with the constant thickness scaling laws[25] as earlier described.) The edge displacements have little effect on the stresses except near the support, where there are sharp deviations from the unperturbed state in opposite directions for out- and inward perturbations. However, for inward edge motion this effect is mitigated by wrinkling, which does not permit the stresses to drop below zero (Fig. 4). The associated shape plots reveal that the central membrane regions (where the stresses are virtually unchanged) undergo axial displacements with little distortion.

This kinematic pattern is seen even better if, rather than the shapes, their axial differences from the undisturbed states are plotted, as in Fig. 5 for three membrane dishes. (Figures 3 and 4 correspond in the second plot to the third curves from the positive and negative extremes of ΔR.) These results, which are representative of the entire study, show that 1) the magnitude of the shape errors is smaller for deeper dishes and 2) the edge effect spreads to the center in a sufficiently shallow dish. The latter phenomenon, which marks a diminishing unaffected zone, becomes more pronounced with an increased pressurization level (load cases 250–1000) and with greater magnitudes of the edge perturbation.

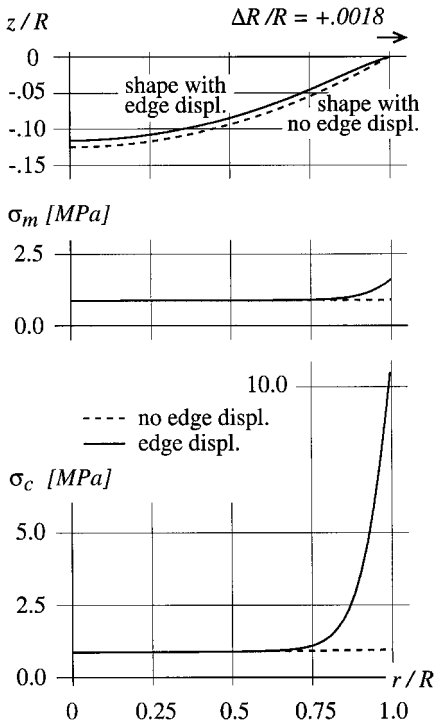

Fig. 3 Boundary-layer effect for $f/D = 1$ membrane paraboloid, load case 125, from an outward edge displacement of $\Delta R/R = +0.0018$ (equivalent to $-150°C$ temperature change).

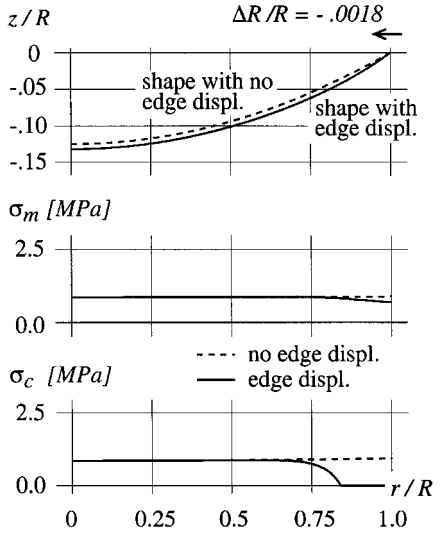

Fig. 4 Boundary-layer effect for $f/D = 1$ membrane paraboloid, load case 125, from an inward edge displacement of $\Delta R/R = -0.0018$ (equivalent to +150°C temperature change).

One way to eliminate the adverse effect of edge perturbations on reflector accuracy is to involve only the center of the dish in the rf operation. This region can be conveniently defined via the uniformity of the error functions in Fig. 5. Thus the unaffected zone is taken to be the region where the axial displacements differ from that at the apex with less than a fraction φ of the latter (cf. Fig. 6); φ arbitrarily selected in the present study as 0.001. (Varying φ within the [0.0005, 0.01] range did not influence the observations discussed in the following.)

How R_0 depends on the studied parameters is shown in Fig. 7. To illustrate the meaning of the plots, consider the example of Fig. 3. The R_0/R value for this model can be read from the $f/D = 1.0$

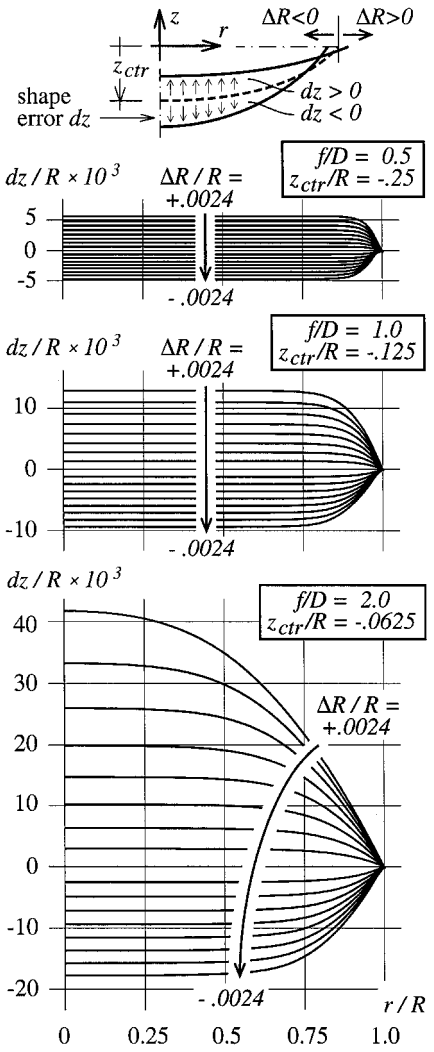

Fig. 5 Changes of three parabolic shapes for the studied edge displacements, load case 125 (ΔR varies in 16 even steps).

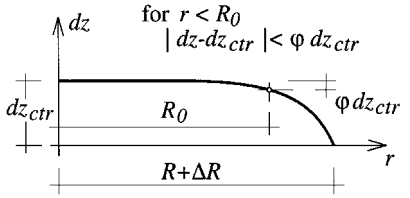

Fig. 6 Definition of the unaffected center radius R_0 via the tolerance φ.

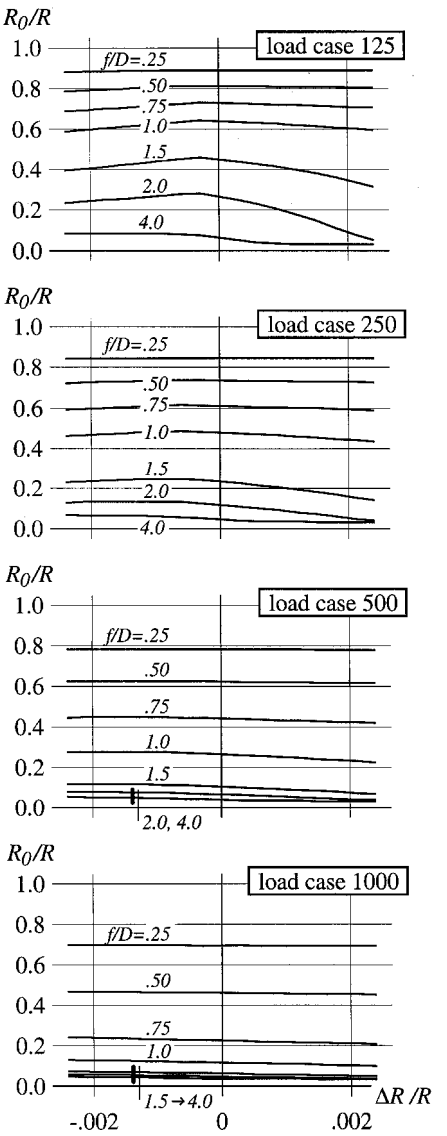

Fig. 7 Size of the region not involved in the boundary-layer effect as a function of dish shape and edge perturbations.

curve in Fig. 7 as $R_0/R \approx 0.61$ (load case 125, $\Delta R/R = +0.0018$). This value marks a location in Fig. 3 slightly inward from where the responses of the unperturbed and perturbed membranes can be visually discerned.

Two characteristics of the plots in Fig. 7 caused by the current axial error-based definition of R_0 need to be commented upon: 1) the R_0/R values on the vertical axes (no support perturbation) can be realized only in the limit $\Delta R \to 0$, and 2) R_0 cannot fully disappear even if the shape of the entire dish is altered. It is the latter phenomenon that results in the congestion of the curves for the shallower dishes and for intense pressures at values slightly above the abscissa axes even though no region of the film is left unaffected in these cases. Nevertheless, the measure based on shape errors is preferred here because 1) shape errors are associated with reflector accuracy and 2) the highlighted spurious behavior of the plots is localized to regions of unlikely practical interest.

The plots reveal the following:

1) The unaffected zone diminishes with a) increasing f/D ratios (shallow dishes) and b) high pressures.

2) For deep dishes and for high pressure levels, R_0 is independent of both the direction and the magnitude of the edge perturbations.

3) For moderately deep to shallow dishes ($f/D = 1.0$ and up), R_0 depends on the magnitude of the perturbations slightly if the latter entail inward edge motion ($\Delta R < 0$) and strongly if the edge is moved outward ($\Delta R > 0$).

Wrinkling

The mechanics of film structures is profoundly affected by the presence (or the lack of) wrinkling, as seen in Figs. 3 and 4. However, because of the associated numerical difficulties and/or the limitations of many commercial FEM codes wrinkling is often ignored, and localized compressive stresses are tolerated. Associated shape prediction errors for the entire dish (not just the unaffected zone studied in the preceding section) are shown in Table 3 for an edge perturbation corresponding to a moderate $\Delta T = 50°C$ temperature increase (cf. Fig. 4).

The shallower the dish and the lower the pressurization level, the greater the errors. For the 125-load case the errors reach the guideline tolerance at $f/D = 1$, and they quickly become excessive beyond. The impact of the dish shape appears to be similarly dramatic for higher pressures, too, but the dish shapes associated with the onset of wrinkling are increasingly shallow.

Table 3 Normalized shape prediction errors $e = (e_{eu} \times 10^4/R)$ caused by unmodeled wrinkling, load cases 125–1000, uniform +50°C temperature increase (no target f/D ratio identifies the initially flat membranes)

f/D	0.25	0.50	0.75	1.0	1.5	2.0	4.0	n/a[a]
125	0.1	0.2	0.5	0.7	1.3	2.0	4.7	17
250	——	0.0	0.1	0.1	0.3	0.4	1.1	6.7
500	——	——	——	——	——	——	0.0	1.5
1000	——	——	——	——	——	——	——	0.3

[a]n/a, Not applicable.

Conclusions

The sensitivity of shapes and shape predictions to selected effects have been explored and evaluated for axisymmetric precision membrane antennas in the context of currently considered rf applications. It has been demonstrated that failure to properly account for 1) limited deviations from nominal film properties, 2) moderate thermal effects, and 3) wrinkling introduce errors into the results that can render the shape prediction inappropriate for precision antenna design. The practical significance of the boundary-layereffect as a possible means to protect a dish center from the deleterious influence of support perturbations has been quantitatively examined. It has been seen that the shallower a membrane dish and the higher the pressure the more sensitive it is to modeling approximations and physical perturbations.

The presented results have been produced with the software package AM for the efficient and high-precisionanalysis of axisymmetric membranes, including wrinkling. The problem formulation embedded in AM has also been reviewed.

Acknowledgments

The present work has been supported by NASA Jet Propulsion Laboratory. General technical direction was provided by Robert E. Freeland.

References

[1]Freeland, R. E., Bilyeu, G., Veal, G. R., and Mikulas, M. M., "Inflatable Deployable Space Structures Technology Summary," International Astronautical Federation, Paper 98-I.5.01, Sept.–Oct. 1998.

[2]Freeland, R. E., and Bilyeu, G., "IN-STEP Inflatable Antenna Experiment," International Astronautical Federation, Paper 92-0301, Aug.–Sept. 1992.

[3]Hencky, H., "Über Den Spannungszustand in Kreisrunden Platten Mit Verschwindender Biegungssteifigkeit," *Zeitschrift für Mathematik und Physik*, Vol. 63, 1915, pp. 311–317.

[4]Libai, A., and Simmonds, J. G., *The Nonlinear Theory of Elastic Shells*, 2nd ed., Cambridge Univ. Press, Cambridge, England, U.K., 1998, pp. 159–341, 389–448.

[5]Campbell, J. D., "On the Theory of Initially Tensioned Circular Membranes Subjected to Uniform Pressure," *Quarterly Journal of Mechanics and Applied Mathematics*, Vol. 9, Pt. 1, 1956, pp. 84–93.

[6]Beck, A., and Grabmüller, H., "Wrinkle-Free Solutions in the Theory of Curved Circular Membranes," *Journal of Engineering Mathematics*, Vol. 27, No. 4, 1993, pp. 389–409.

[7]Fichter, W. B., "Some Solutions for the Larger Deflections of Uniformly Loaded Circular Membranes," NASA TP 3568, July 1997.

[8]Baginski, F., Collier, W., and Williams, T., "A Parallel Shooting Method for Determining the Natural Shape of a Large Scientific Balloon," *SIAM Journal on Applied Mathematics*, Vol. 58, No. 3, 1998, pp. 961–974.

[9]Joshi, S. P., and Murphy, L. M., "Large Axisymmetric Deformation for a Laminated Composite Membrane," *Journal of Applied Mechanics*, Vol. 57, No. 1, 1990, pp. 150–157.

[10]Shaw, F. S., and Perrone, N., "A Numerical Solution for the Nonlinear Deflection of Membranes," *Journal of Applied Mechanics*, Vol. 21, No. 2, 1954, pp. 117–128.

[11]Haseganu, E. M., and Steigmann, D. J., "Analysis of Partly Wrinkled Membranes by the Method of Dynamic Relaxation," *Computational Mechanics*, Vol. 14, No. 6, 1994, pp. 596–614.

[12]Palisoc, A. L., and Huang, Y., "Design Tool for Inflatable Space Structures," AIAA Paper 97-1378, April 1997.

[13]Taylor, Sir G. I., "On the Shapes of Parachutes," *The Scientific Papers of Sir G. I. Taylor*, edited by G. K. Batchelor, Vol. 3, Cambridge Univ. Press, Cambridge, England, U.K., 1963, pp. 26–37.

[14]Wu, C. H., "The Wrinkled Axisymmetric Air Bags Made of Inextensible Membrane," *Journal of Applied Mechanics*, Vol. 41, No. 4, 1974, pp. 963–968.

[15]Palisoc, A., Veal, G., Greschik, G., and Mikulas, M., "Geometry Attained by Pressurized Membranes," *Space Telescopes and Instruments V*, Vol. 3356, Society of Photo-Optical Instrumentation Engineers, Kona, HI, 1998, pp. 747–757.

[16]Vaughan, H., "Pressurizing a Prestretched Membrane to Form a Paraboloid," *International Journal of Engineering Science*, Vol. 187, No. 1, 1980, pp. 99–107.

[17]Greschik, G., Palisoc, A., and Mikulas, M. M., "Approximations and Errors in Pressurized Axisymmetric Membrane Shape Predictions," AIAA Paper 98-2101, April 1998.

[18]Greschik, G., Palisoc, A., Veal, G., Cassapakis, C., and Mikulas, M. M., "Approximating Paraboloids with Axisymmetric Pressurized Membranes," AIAA Paper 98-2102, April 1998.

[19]Bromberg, E., and Stoker, J. J., "Non-Linear Theory of Curved Elastic Sheets," *Quarterly of Applied Mathematics*, Vol. 3, No. 3, 1945, pp. 246–265.

[20]Wan, F. Y. M., and Weinitschke, H. J., "Boundary Layer Solutions for Some Non-Linear Elastic Membrane Problems," *Zeitschrift für Angewandte Mathematik und Physik*, Vol. 38, No. 1, 1987, pp. 79–91.

[21]Stein, M., and Hedgepeth, J. M., "Analysis of Partly Wrinkled Membranes," NASA TN D-813, July 1961.

[22]Wu, C. H., "Nonlinear Wrinkling of Nonlinear Membranes of Revolution," *Journal of Applied Mechanics*, Vol. 45, No. 3, 1978, pp. 533–538.

[23]Murphy, L. M., "Moderate Axisymmetric Deformations of Optical Membrane Surfaces," *Journal of Solar Energy Engineering*, Vol. 109, No. 2, 1987, pp. 111–120.

[24]Ruze, J., "Antenna Tolerance Theory—a Review," *Proceedings of the IEEE*, Vol. 54, No. 4, 1966, pp. 633–640.

[25]Greschik, G., and Mikulas, M. M., "Scale Model Testing of Nonlinear Phenomena with Emphasis on Thin Film Deployable Structures," *Symposium on Deployable Structures: Theory and Applications*, Kluwer Academic (to be published).

[26]Greschik, G., Mikulas, M. M., and Freeland, R. E., "The Nodal Concept of Deployment and the Scale Model Testing of Its Application to a Membrane Antenna," AIAA Paper 99-1523, April 1999.

S. Saigal
Associate Editor